INSTITUTE OF PHYSICS PUBLISHING JOURNAL OF PHYSICS: CONDENSED MATTER

J. Phys.: Condens. Matter **13** (2001) 4789–4800 www.iop.org/Journals/cm PII: S0953-8984(01)22183-3

Isotropic–nematic interfaces of hard-rod fluids

Kostya Shundyak and René van Roij[1]

Institute for Theoretical Physics, Utrecht University, Princetonpln 5, 3584 CC Utrecht, The Netherlands

Received 21 February 2001

Abstract

Within the Onsager theory we study the planar isotropic–nematic interface of fluids of hard rods. We present a method with which interfacial biaxiality can be dealt with efficiently and systematically, and apply it (i) to the pure hard-rod fluid and (ii) to a binary mixture of thin and thick hard rods. In the one-component system we find a surface tension that is lower by 15% than earlier estimates, and monotonic profiles of the density and the uniaxial order parameter. The biaxial order parameter profile is non-monotonic. In the two-component system we find the possibility of non-monotonic density profiles, and a maximum in the surface tension as a function of the pressure.

1. Introduction

The experimental observation of a concentration-driven transition from an isotropic fluid to an anisotropic fluid phase in suspensions of rod-like particles dates back to the 1920s and 1930s [1, 2]. The distinction between the low-density isotropic phase and the high-density nematic phase is the broken rotation symmetry in the latter; the rods in the bulk nematic phase point, on average, along a specific direction, say $\hat{n}$, in space. The theoretical explanation of this symmetry-breaking transition was given in the 1940s by Onsager [3], who modelled the rods as *hard* rods and showed that the free volume per particle (i.e. a measure for the 'packing entropy') is maximal in the nematic phase, while the orientation entropy is maximal in the isotropic phase. The competition between these two contributions to the total entropy is such that the system is in the isotropic phase at low enough density $n < n_I$, and in the nematic phase at high enough density $n > n_N$. Co-existence of an isotropic phase (at density n_I) and nematic phase (at density n_N) takes place when $n_I < n < n_N$. In this case the system is *inhomogeneous*, and exhibits an interface that separates the co-existing bulk phases. Several authors [4–12] considered a generalization of Onsager's theory to include inhomogeneities in order to study the isotropic–nematic interface. An important issue that appears in these studies involves the numerical value of the surface tension as a function of the angle between the interface normal $\hat{z}$ and the (imposed) nematic director $\hat{n}$ far from the interface. Another issue concerns the equilibrium profile of the total density and the orientation order parameters as a function of the spatial coordinate z running across the interface. In particular, Chen's

[1] Corresponding author.

work in 1993 [7] seems to settle that (i) the lowest interfacial tension is obtained when $\hat{n} \perp \hat{z}$, (ii) the density and uniaxial order parameter profile are monotonic functions of z, (iii) the biaxial order parameter profile is small in magnitude and ignoring it (in order to reduce the computational cost) hardly affects the numerical value of the tension. Recently, however, some of these findings were challenged in [8], where it was argued that the equilibrium profiles are non-monotonic and that the tension is higher, by about 50%, than reported by Chen [7]. This is one reason why we revisit the problem here.

The other reason why we study the inhomogeneous pure hard-rod fluid is due to its role as a stepping stone towards the study of interfacial phenomena in *binary mixtures* of hard rods. To the best of our knowledge the interfaces of these systems have not been studied at all, but the extremely rich phenomenology that occurs in *bulk* mixtures is expected to have interesting repercussions for their interface properties. For instance, a bulk mixture of rods of different lengths was shown to exhibit a strong fractionation at the isotropic–nematic phase boundary [13, 14], a nematic–nematic immiscibility gap with interesting critical (consolute) point properties, and an isotropic–nematic–nematic triple point [15–18]. Binary mixtures of thick and thin rods exhibit qualitatively similar features, with a bulk isotropic–isotropic co-existence regime in between a critical point at low pressures and an isotropic–isotropic–nematic triple point at higher pressures, provided the diameter ratio of the two species is large enough [19–21]. It is to be expected that the presence of critical and triple points in the bulk phase diagrams leads to interesting wetting and capillary effects. Here we report some of our first findings on the free isotropic–nematic interface of mixtures of thick and thin hard rods.

This paper is organized as follows. In section 2 we formulate the generalized Onsager theory for a pure system of hard rods. Although the density functional formalism we adopt does not differ from that in previous studies, our numerical implementation does differ somewhat. In particular our perturbative treatment of the biaxiality that occurs in the interface is supposed to be rather efficient. We calculate the equilibrium profiles and the tension of the free isotropic–nematic interface for $\hat{n} \perp \hat{z}$. In section 3 we sketch the extension of the theory to binary mixtures of rods of different diameters. In section 4 we discuss these results, and present an outlook to future work.

2. The one-component fluid

2.1. Density functional

Consider a one-component system of hard spherocylinders of length L and diameter D in a macroscopic volume V at temperature T and chemical potential μ. The thermodynamics and the structure of this fluid can be described by a functional $\Omega[\rho]$ of the one-particle distribution function $\rho(\boldsymbol{r}, \hat{\omega})$, where $\boldsymbol{r}$ denotes the centre-of-mass coordinate of the rods and $\hat{\omega}$ the orientation of the long axis. The density functional $\Omega[\rho]$ is such that (i) it is minimized, for given (μ, V, T), by the equilibrium one-particle distribution, and (ii) the minimal value of the functional is the equilibrium grand potential [22]. Here we use the Onsager functional, which in the absence of an external potential is given by

$$\beta\Omega[\rho] = \int \mathrm{d}\boldsymbol{r}\mathrm{d}\hat{\omega}\rho(\boldsymbol{r}, \hat{\omega})\Big(\log[\rho(\boldsymbol{r}, \hat{\omega})L^2 D] - 1 - \beta\mu\Big) - \frac{1}{2}\int \mathrm{d}\boldsymbol{r}\mathrm{d}\hat{\omega}\mathrm{d}\boldsymbol{r}'\mathrm{d}\hat{\omega}' f(\boldsymbol{r}, \hat{\omega}; \boldsymbol{r}', \hat{\omega}')\rho(\boldsymbol{r}, \hat{\omega})\rho(\boldsymbol{r}', \hat{\omega}') \tag{1}$$

with $\beta = 1\ (\mathrm{kT})^{-1}$, and f the Mayer function which equals -1 if the rods overlap and 0 otherwise [3,23]. Although the functional of equation (1) is a second virial approximation, i.e.

cubic and higher order terms in ρ are being ignored, it is supposed to give accurate results for rods in the 'needle' limit $L/D \to \infty$ [3,23]. In this paper we will adopt this limit throughout. The minimum condition on the functional, $\delta\Omega[\rho]/\delta\rho(\boldsymbol{r}, \hat{\omega}) = 0$, leads to the nonlinear integral equation

$$\log[\rho(\boldsymbol{r}, \hat{\omega})L^2 D] - \int \mathrm{d}\boldsymbol{r}' \mathrm{d}\hat{\omega}' f(\boldsymbol{r}, \hat{\omega}; \boldsymbol{r}', \hat{\omega}')\rho(\boldsymbol{r}', \hat{\omega}') = \beta\mu \tag{2}$$

to be solved for the equilibrium distribution $\rho(\boldsymbol{r}, \hat{\omega})$. Once $\rho(\boldsymbol{r}, \hat{\omega})$ has been determined, it can be inserted into the functional to obtain the minimum value

$$\beta\Omega_{min} = \int \mathrm{d}\boldsymbol{r}\mathrm{d}\hat{\omega}\rho(\boldsymbol{r}, \hat{\omega})\Big(-1 + \frac{1}{2}\log[\rho(\boldsymbol{r}, \hat{\omega})L^2 D] - \frac{1}{2}\beta\mu\Big). \tag{3}$$

Note that $\Omega_{min} = -pV$ for a bulk system in a volume V, with $p = p(\mu, T)$ the pressure. In the presence of a surface or interface of area A we have $\Omega_{min} = -pV + \gamma A$ with $\gamma = \gamma(\mu, T)$ the surface or interface tension.

2.2. The bulk isotropic and nematic phase

The *bulk* isotropic and nematic phases are both homogeneous, and hence the corresponding equilibrium distributions are of the form $\rho(\boldsymbol{r}, \hat{\omega}) = \rho(\hat{\omega})$. The stationarity equation (2) then reduces to

$$\log[\rho(\hat{\omega})L^2 D] + \int \mathrm{d}\hat{\omega}' E(\hat{\omega}, \hat{\omega}')\rho(\hat{\omega}') = \beta\mu \tag{4}$$

with E the excluded volume of a pair of spherocylinders given by

$$E(\hat{\omega}, \hat{\omega}') = -\int \mathrm{d}\boldsymbol{r}' f(\boldsymbol{r}, \hat{\omega}, \boldsymbol{r}', \hat{\omega}') = 2L^2 D|\sin\gamma| \tag{5}$$

in terms of the angle γ between $\hat{\omega}$ and $\hat{\omega}'$, i.e. $\cos\gamma = \hat{\omega}\cdot\hat{\omega}'$. Solutions to equation (4) have been studied in full detail over the years; here we give a brief overview of results needed and used in this work. It is convenient to write $\rho(\hat{\omega}) = n\psi(\hat{\omega})$, with $n = \int \mathrm{d}\hat{\omega}\rho(\hat{\omega})$ the number density, and $\psi(\hat{\omega}) = \rho(\hat{\omega})/n$ the orientation distribution function. At low enough values of $\beta\mu$ the only solution for $\rho(\hat{\omega})$ is the isotropic distribution, with $\psi(\hat{\omega}) = \psi_I = (4\pi)^{-1}$ and n determined uniquely by $\beta\mu$ through $\log[nL^2 D/(4\pi)] + (\pi/2)L^2 Dn = \beta\mu$. At sufficiently high $\beta\mu$ the isotropic distribution is unstable with respect to orientational ordering of uniaxial symmetry [24], and the distribution resulting from equation (4) is then anisotropic, i.e. peaked in the direction of nematic director $\hat{n}$. The functional form of the nematic distribution $\psi(\hat{\omega})$ is not known analytically, but is easily obtained by solving equation (4) numerically (at high enough $\beta\mu$). The bulk nematic phase is of uniaxial symmetry, i.e. $\psi(\hat{\omega}) = \psi(\theta)$, with θ the polar angle of $\hat{\omega}$ with respect to the symmetry axis $\hat{n}$ [3,23]. Due to up-down symmetry we have $\psi(\theta) = \psi(\pi - \theta)$, so that the numerical determination of $\psi(\theta)$ need only be performed for $\theta \in [0, \pi/2]$. The nematic distribution, as follows from equation (4), is calculated on an equidistant θ-grid with N_θ points $\theta_i \in [0, \pi/2]$, where $1 \leqslant i \leqslant N_\theta$. Using $N_\theta = 200$, and the analytic expression $\psi_I = (4\pi)^{-1}$ for the isotropic orientation distribution, one finds bulk phase co-existence of an isotropic phase of density n_I and a nematic phase of density n_N and orientation distribution $\psi_N(\theta)$ at $\beta\mu = \beta\mu_{IN} = 5.4815$, with $n_I L^2 D = 4.189$ and $n_N L^2 D = 5.336$. The degree of orientational ordering is characterized by the standard (uniaxial) nematic order parameter $S = \langle P_2(\cos\theta)\rangle$, which takes the value $S = 0$ in the isotropic phase and $S = 0.7922$ in the co-existing nematic phase [23].

Unfortunately we cannot use these literature values for the bulk IN co-existence in the study of the IN interface. The reason is that the two phases must be treated on the same footing

in the study of the interface, whereas the method with which the bulk values are obtained is different in the two phases: the isotropic distribution is treated analytically, and the nematic distribution numerically on a θ-grid. Moreover, the number of $N_\theta = 200$ grid points is too large to be combined with spatial inhomogeneity. For that reason we chose to calculate the IN bulk co-existence based on distribution functions that we determine numerically on an equidistant θ-grid of $N_\theta = 50$ grid points in *both* the isotropic and the nematic phase. The resulting bulk IN co-existence data are $\beta\mu_{IN} = 5.4744$, $n_I L^2 D = 4.185$, $n_N L^2 D = 5.327$, and the co-existing order parameters are $S_I = 0.0029$ and $S_N = 0.7915$. Obviously these data differ somewhat from the literature values given above, but the differences are small. The fact that $S_I \neq 0$ exactly is a harmless, purely numerical effect without any physical consequence since $S_I \ll 1$. These numerical values will be used in the study of the IN interface.

2.3. The free isotropic–nematic interface

We proceed and deal with the properties of the interface between the co-existing isotropic and the nematic phase. We assume this interface to be flat, with surface normal $\hat{z}$. The one-particle distribution, which in this geometry depends on the coordinate $z = \boldsymbol{r} \cdot \hat{z}$ and the orientation $\hat{\omega}$, is a solution of the stationarity equation (2), with $\mu = \mu_{IN}$,

$$\log[\rho(z, \hat{\omega})L^2 D] + \int \mathrm{d}z' \mathrm{d}\hat{\omega}' K(z - z'; \hat{\omega}, \hat{\omega}')\rho(z', \hat{\omega}') = \beta\mu_{IN} \tag{6}$$

subject to the boundary conditions

$$\begin{aligned} &\rho(z, \hat{\omega}) = n_I \psi_I \qquad (z \to -\infty) \\ &\rho(z, \hat{\omega}) = n_N \psi_N(\arccos(\hat{\omega} \cdot \hat{n})) \qquad (z \to \infty). \end{aligned} \tag{7}$$

Here $\hat{n}$ is a fixed nematic director at $z \to \infty$. In equation (6) we defined the kernel K as

$$K(z - z', \hat{\omega}, \hat{\omega}') = -\int \mathrm{d}x' \mathrm{d}y' f(\boldsymbol{r}, \hat{\omega}; \boldsymbol{r}', \hat{\omega}') \tag{8}$$

which was calculated explicitly for hard spherocylinders of arbitrary L/D in [25]. In the limit $L/D \to \infty$ of interest here the results obtained in [25] can be written as

$$K(z_{12}, \hat{\omega}_1, \hat{\omega}_2) = \begin{cases} 0 & |z_{12}| > |A| + |B| \\ \dfrac{E(\hat{\omega}_1, \hat{\omega}_2)}{4|AB|}(|A| + |B| - |z_{12}|) & |A| - |B| \leqslant |z_{12}| \leqslant |A| + |B| \\ \dfrac{E(\hat{\omega}_1, \hat{\omega}_2)}{2|A|} & |z_{12}| \leqslant |(|A| - |B|)| \end{cases} \tag{9}$$

with the excluded volume E defined in equation (5) and $A = \frac{L}{2}\max(\hat{\omega}_1 \cdot \hat{z}, \hat{\omega}_2 \cdot \hat{z})$ and $B = \frac{L}{2}\min(\hat{\omega}_1 \cdot \hat{z}, \hat{\omega}_2 \cdot \hat{z})$.

Note that the profiles that satisfy equations (6)–(8) depend nontrivially on $\hat{n} \cdot \hat{z}$. In all cases where $\hat{n}$ is not parallel to $\hat{z}$, the uniaxial symmetry about $\hat{n}$ is broken in the interface, i.e. the distribution is a nontrivial function of the spatial coordinate z, the polar angle θ *and* the azimuthal angle φ of the orientation $\hat{\omega}$ with respect to $\hat{n}$. Taking into account inhomogeneity and biaxiality simultaneously is computationally demanding, and therefore approximations that simplify or discard either one or both of these features have often been made. Instead of solving the Euler–Lagrange equations (6)–(8), some authors treated the problem variationally by e.g. imposing a step function for the total density [4], or a wider class of variational smooth profiles with a finite width [5, 6]. It was argued and shown by Chen and Noorlandi [6], and by Chen [7], who did solve the full Euler–Lagrange equations (6)–(8) numerically on a (z, θ, φ) grid, that the biaxiality of the interface profile is small and that it does not affect the numerical

value of the surface tension γ within the numerical accuracy. The results of [7] seem to settle that the lowest tension is obtained when $\hat{n} \perp \hat{z}$, that its numerical value is given by $\beta\gamma LD = 0.181 \pm 0.002$, and that the profile of the total density and the uniaxial nematic order parameter are monotonic functions of the spatial variable z. Very recently, however, it was argued by Koch and Harlen [8] that a refinement of the z-grid yields a nonmonotonic density profile, and a significantly higher surface tension than that determined in [7]. This is one of the reasons why we revisit the problem here, as already stated in the introduction.

Since there is no disagreement in the literature on the conclusion that the surface tension is minimal when $\hat{n} \perp \hat{z}$, we take this for granted here, and thus only consider the geometry where $\hat{n} \perp \hat{z}$. We define the polar and azimuthal angle θ and φ of $\hat{\omega}$ by $\cos\theta = \hat{n} \cdot \hat{\omega}$ and $\sin\theta \sin\varphi = \hat{z} \cdot \hat{\omega}$. This choice for the angles θ and φ is identical to that in [7], and is such that the one-particle distribution can exactly be written as the $N \to \infty$ limit of

$$\rho(z, \theta, \varphi) = \sum_{j=0}^{N} \rho_j(z, \theta) \cos(2j\varphi). \tag{10}$$

The distribution is thus characterized by the functions $\rho_j(z, \theta)$. On the basis of the small biaxiality reported by Chen [7] we expect that $|\rho_j(z, \theta)|$ rapidly decreases for increasing j, so that accurate distributions are obtained for small N. Insertion of the parameterization (10) into the stationarity condition (6) yields, after multiplication equation (6) by $\cos(2k\varphi)$ and integration from $\varphi = 0$ to $\varphi = 2\pi$ that

$$\beta\mu_{IN}\delta_{k0} = \frac{1}{2\pi}\int_0^{2\pi} \mathrm{d}\varphi \cos(2k\varphi) \log[\sum_{j=0}^{N} \rho_j(z, \theta) \cos(2j\varphi) L^2 D] + \int \mathrm{d}z' \int \mathrm{d}\theta' \sin\theta' \sum_{m=0}^{N} K_{km}(z - z', \theta, \theta')\rho_m(z', \theta') \qquad (k = 0, 1, \ldots N) \tag{11}$$

where the doubly azimuthally integrated kernels K_{km}, with $k, m = 0, 1, \ldots N$, are given by

$$K_{km}(z - z', \theta, \theta') = \frac{1}{2\pi}\int_0^{2\pi} \mathrm{d}\varphi \int_0^{2\pi} \mathrm{d}\varphi' \cos(2k\varphi) \cos(2m\varphi') K(z - z', \hat{\omega}, \hat{\omega}'). \tag{12}$$

For a given value of N, equation (11) constitutes $N+1$ coupled nonlinear integral equations for the $N+1$ unknowns $\rho_k(z, \theta)$, $(k = 0, 1, \cdots N)$. This set of equations can be solved numerically on a (z, θ) grid, e.g. by iteration. Note that the numerical determination of the K_{km}'s, on a $(z - z', \theta, \theta')$ grid, need be performed only once, as it does not depend on $\rho_j(z, \theta)$.

By setting $N = 0$ we ignore any biaxiality in the interface, i.e. only the term $j = 0$, which is independent of φ, contributes in equation (10). The resulting equilibrium distribution $\rho_0(z, \theta)$ is, from equation (11), the solution of

$$\beta\mu_{IN} = \log[\rho_0(z, \theta) L^2 D] + \int \mathrm{d}z' \int \mathrm{d}\theta' \sin\theta' K_{00}(z - z', \theta, \theta')\rho_0(z', \theta'). \tag{13}$$

This is, essentially, the equation solved by Chen and Noorlandi in [6] on an equidistant grid (z_i, θ_j), with $N_z = 40$ points $z_i \in [-5L, 5L]$ and $N_\theta = 41$ points $\theta \in [0, \pi/2]$, i.e. the resolution is such that $z_{i+1} - z_i = L/4$ and $\theta_{j+1} - \theta_j = \pi/80$. The profiles reported in [6] are monotonic, and the surface tension γ for the case of interest here, $\hat{n} \perp \hat{z}$, is given by $\beta\gamma LD = 0.183 \pm 0.002$ [6,7]. When we solve this equation on approximately the same grid as that of [6,7], i.e. with $N_\theta = 50$ and $N_z = 40$, we obtain the value $\beta\gamma LD = 0.187 \pm 0.001$, where the uncertainty is estimated on the basis of the accuracy of the numerical φ integrations in the calculation of K_{00}. A refinement of the θ grid, i.e. increasing N_θ, does not change the

value of γ within the numerical accuracy. However, gradually increasing N_z from 40 to 500 (with the same interval $z_i \in [-5L, 5L]$) lowers γ systematically. This can be seen in figure 1, where we plot γ as a function of $1/M$ with fixed $N_\theta = 50$, where $M = N_z/10$ is the number of grid points per rod length L (in the interval $z_i \in [-5L, 5L]$). On the basis of this figure we conclude that the calculation with $M = 50$ has converged, and yields $\beta\gamma LD = 0.156 \pm 0.001$, which is about 15% lower than the estimate given in [6, 7]. The uniaxially symmetric profiles are monotonic, in agreement with [6, 7]. However, these findings are in disagreement with the claims in [8], where a refinement of the spatial grid yields a higher value for γ and a nonmonotonic density profile.

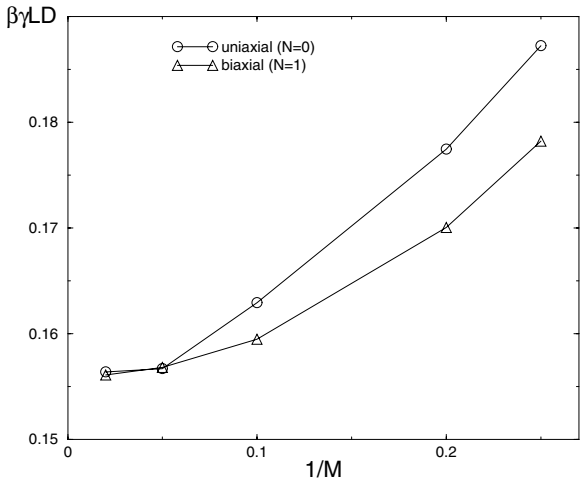

Figure 1. Surface tension γ of the free planar isotropic–nematic interface of hard rods of length L and diameter $D \ll L$ as a function of M^{-1}, where M is the number of spatial grid-points per L (see text). For both curves the bulk nematic director is perpendicular to the interface normal. The interface biaxiality is ignored in the $N = 0$ curve ($\circ$), and taken into account to lowest order in the $N = 1$ curve ($\triangle$). The significant levelling of the two curves for $M \geqslant 20$ indicates good convergence for the $M = 50$ grid.

In order to study the effect of interfacial biaxiality we consider the Euler–Lagrange equations (11) for $N = 1$, which we write as

$$\begin{aligned}\beta\mu_{IN} &= \log[\rho_0(z,\theta)L^2D] + I_0\left(\frac{\rho_1(z,\theta)}{\rho_0(z,\theta)}\right) \\ &\quad + \int \mathrm{d}z'\mathrm{d}\theta' \sin\theta' \big(K_{00}(z-z',\theta,\theta')\rho_0(z',\theta') + K_{01}(z-z',\theta,\theta')\rho_1(z',\theta')\big) \\ 0 &= I_1\left(\frac{\rho_1(z,\theta)}{\rho_0(z,\theta)}\right) + \int \mathrm{d}z'\mathrm{d}\theta' \sin\theta' \big(K_{10}(z-z',\theta,\theta')\rho_0(z',\theta') \\ &\quad + \ K_{11}(z-z',\theta,\theta')\rho_1(z',\theta')\big)\end{aligned} \tag{14}$$

where $I_0(x)$ and $I_1(x)$ are defined, for $|x| < 1$, as

$$\begin{aligned} I_0(x) &= \frac{1}{2\pi}\int_0^{2\pi} \mathrm{d}\varphi \log\big(1 + x\cos(2\varphi)\big) = \log\frac{1+\sqrt{1-x^2}}{2} \\ I_1(x) &= \frac{1}{2\pi}\int_0^{2\pi} \mathrm{d}\varphi \cos(2\varphi)\log\big(1 + x\cos(2\varphi)\big) = \frac{1-\sqrt{1-x^2}}{x}. \end{aligned} \tag{15}$$

Equation (14), with the boundary conditions given in equation (7), can be solved iteratively on a (z, θ) grid. Note that the boundary conditions given in equation (7) imply that $\rho_1(z, \theta) \to 0$ for $|z| \to \infty$. From the solution of equation (14) we construct the profile of the total density $\rho(z) = \int \mathrm{d}\hat{\omega}\rho(z, \hat{\omega})$, the uniaxial nematic order parameter $S(z) = \frac{1}{2}\langle 3\cos^2\theta - 1\rangle(z)$, and the biaxiality $\Delta(z) = \langle \frac{3}{2}\sin^2\theta\cos 2\varphi\rangle(z)$. Note that the latter coincides with Chen's definition of biaxiality in [7]. Combining this with our $N = 1$ parameterization of the distribution we obtain

$$\Delta(z) = \frac{\int \mathrm{d}\hat{\omega}\rho(z, \hat{\omega})\frac{3}{2}\sin^2\theta\cos(2\varphi)}{\int \mathrm{d}\hat{\omega}\rho(z, \hat{\omega})} = \frac{3}{4}\frac{\int_0^{\pi/2}\mathrm{d}\theta\sin^3\theta\rho_1(z, \theta)}{\int_0^{\pi/2}\mathrm{d}\theta\sin\theta\rho_0(z, \theta)}. \tag{16}$$

The profiles $\rho(z)$ and $S(z)$ are almost identical to the ones obtained with the uniaxially symmetric profile, and the resulting $\Delta(z)$ is shown in figure 2 for several choices of the z-grid parameter M. It is seen that $\Delta(z)$ is nonmonotonic, with a positive value at the isotropic side of the interface, a negative value at the nematic side, and a decay to zero in the two bulk phases. The structure of $\Delta(z)$ we obtain is very similar to that obtained by Chen in [7]. The negative dip is basically identical, whereas the positive peak in $\Delta(z)$ is a factor of about two smaller than the result in [7]. Refining the z-grid from $M = 4$ to $M = 5$ yields a substantial change in $\Delta(z)$, while further refinement to $M = 20$ and 50 hardly changes the biaxiality (although it does change the resulting surface tension, see figure 1). These results provide support for truncating the expansion in equation (10) at $N = 1$ without loss of quantitative accuracy. The IN surface tension that follows from the biaxial $N = 1$ profiles is also plotted in figure 1. It is seen that γ obtained from the biaxial profiles are substantially smaller than the corresponding uniaxial ones in the case of the cruder grids with $M < 20$. The difference becomes vanishingly small, however, in the case of the $M = 20$ and $M = 50$ grids. We therefore conclude that $\beta\gamma LD = 0.156 \pm 0.001$ for the Onsager model, and that the total density and uniaxial order parameter profiles are monotonic.

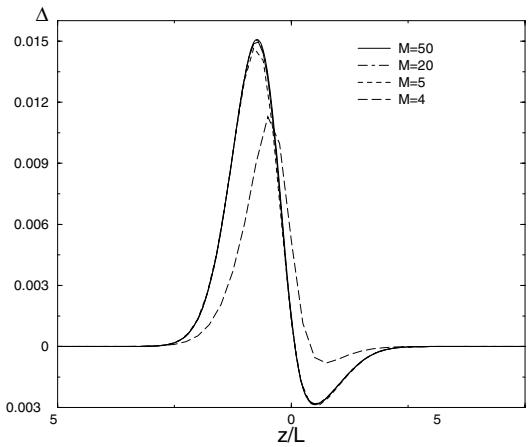

Figure 2. Profile of the biaxial order parameter Δ as a function of the spatial coordinate z running across the isotropic–nematic planar interface for several values of M, the number of grid points per L. The system is isotropic for $z \to -\infty$, and nematic at $z \to \infty$. The $M = 4$ grid is clearly too coarse, and comparing the $M = 20$ and $M = 50$ grid reveals good convergence.

3. Binary mixtures of thick and thin hard rods

3.1. Density functional

We extend the density functional theory formulated in section 2 to the case of a two-component system of hard rods of different diameters, D_1 and D_2, but the same length L. We assume that both rod species are in the needle limit, i.e. $D_1 \ll L$ and $D_2 \ll L$, so that Onsager's second virial theory remains accurate. The ratio of the diameters, $D_2/D_1 \equiv d$, is assumed to be of order unity here, and is the characteristic of the shape difference of the rods. For definiteness we take species 2 to be the thicker species, i.e. $d > 1$. We leave d unspecified for the moment, but will present explicit results for $d = 3$. The grand potential functional of the mixture is written as

$$\beta\Omega[\rho_1, \rho_2] = \sum_{\sigma=1}^{2} \int \mathrm{d}\boldsymbol{r}\mathrm{d}\hat{\omega}\rho_\sigma(\boldsymbol{r}, \hat{\omega})\Big(\log[\rho_\sigma(\boldsymbol{r}, \hat{\omega})L^2 D_\sigma] - 1 - \beta\mu_\sigma \Big) - \frac{1}{2}\sum_{\sigma=1}^{2}\sum_{\sigma'=1}^{2} \int \mathrm{d}\boldsymbol{r}\mathrm{d}\hat{\omega}\mathrm{d}\boldsymbol{r}'\mathrm{d}\hat{\omega}' f_{\sigma\sigma'}(\boldsymbol{r}, \hat{\omega}, \boldsymbol{r}', \hat{\omega}')\rho_\sigma(\boldsymbol{r}, \hat{\omega})\rho_{\sigma'}(\boldsymbol{r}', \hat{\omega}') \tag{17}$$

where $\rho_\sigma(\boldsymbol{r}, \hat{\omega})$ is the one-particle distribution and μ_σ the chemical potential of species $\sigma = 1, 2$. The Mayer function associated with the pair interaction between species σ and σ' is denoted by $f_{\sigma\sigma'}$. The minimum condition $\delta\Omega/\delta\rho_\sigma(\boldsymbol{r}, \hat{\omega}) = 0$ yields the set of nonlinear integral equations for the equilibrium distributions,

$$\log[\rho_\sigma(\boldsymbol{r}, \hat{\omega})L^2 D_\sigma] - \sum_{\sigma'=1}^{2} \int \mathrm{d}\boldsymbol{r}'\mathrm{d}\hat{\omega}' f_{\sigma\sigma'}(\boldsymbol{r}, \hat{\omega}, \boldsymbol{r}', \hat{\omega}')\rho_{\sigma'}(\boldsymbol{r}', \hat{\omega}') = \beta\mu_\sigma. \tag{18}$$

A (formal) insertion of the solutions to equation (18) into the functional Ω leads to the minimum value Ω_{min} given by

$$\beta\Omega_{min} = \sum_{\sigma=1}^{2} \int \mathrm{d}\boldsymbol{r}\mathrm{d}\hat{\omega}\rho_\sigma(\boldsymbol{r}, \hat{\omega})\Big(-1 + \frac{1}{2}\log[\rho(\boldsymbol{r}, \hat{\omega})L^2 D_\sigma] - \frac{1}{2}\beta\mu_\sigma \Big) \tag{19}$$

which is the equilibrium grand potential of the system for given μ_1 and μ_2, i.e. for a given composition. As for the one-component system we have $\Omega_{min} = -pV$ for a bulk system of volume V, with $p(\mu_1, \mu_2, T)$ the pressure. The tension $\gamma(\mu_1, \mu_2, T)$ due to an interface or surface of area A follows from $\Omega_{min} = -pV + \gamma A$.

3.2. Bulk phase diagrams

Several authors studied the homogeneous, $\boldsymbol{r}$-independent, solutions of expressions equivalent to the Euler–Lagrange equations (18), e.g. for the case of rods of different lengths [13, 15–18], or for rods of different diameters [19–21]. The striking features of the phase diagrams that were obtained for thick–thin mixtures are the strong fractionation that associates the isotropic–nematic co-existence, and the possibility for nematic–nematic and isotropic–isotropic demixing if d is large enough. In figure 3 we show the bulk phase diagrams for $d = 3$ in the p-x representation, where p is the pressure and x the mole fraction of the thicker species, i.e. $x = n_2/(n_1{+}n_2)$ with $n_\sigma = \int \mathrm{d}\hat{\omega}\rho_\sigma(\hat{\omega})$ the number density of species σ in the homogeneous fluid. The phase diagram in figure 3, which follows from Ω_{min} using the standard mechanical and chemical equilibrium conditions, is identical to the bulk phase diagrams presented in [21], apart from a very small numerical uncertainty that is invisible on the scale of the plots. The grey area denotes the two-phase region; the pressure-composition representation is such that the tie lines that connect co-existing phases are horizontal. The phase diagram for $d = 3$ in

figure 3 is of the 'spindle' type, and exhibits a fractionation effect whereby the thicker rods have a relatively strong preference for the nematic phase. The reason for this is that their larger excluded volume interactions are more susceptible to orientational ordering. Below we discuss the free isotropic–nematic interfaces associated with the state-points indicated by open circles (○) in figure 3. The calculations should be seen as a stepping stone towards the study of interfaces in more asymmetric mixtures, where triple points and critical points in the phase diagram are expected to show interesting interface phenomena.

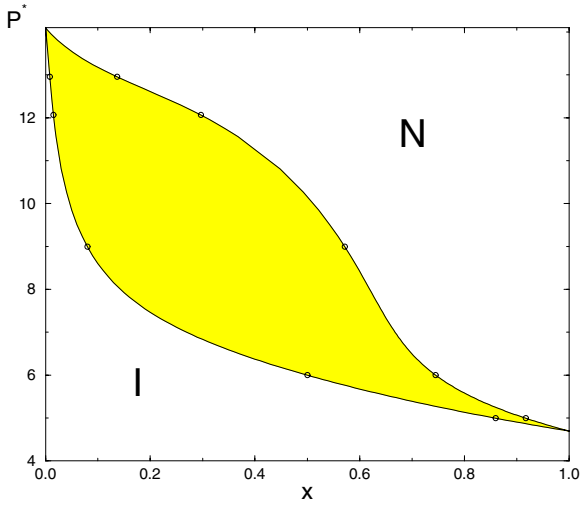

Figure 3. Pressure-composition bulk phase diagram of a binary mixture of thick and thin rods with diameter ratio $D_2/D_1 = 3$. The dimensionless pressure is $p^* = \beta p L^2 D_1$, and x is the mole fraction of thicker rods. The grey area denotes the immiscibility gap between the isotropic phase I and the nematic phase N. We studied the isotropic–nematic interfaces at the states indicated by open circles (○).

3.3. The free isotropic–nematic phase

We consider the interfaces that separate the co-existing isotropic and nematic bulk phases in the binary hard-rod mixtures with diameter ratio $d = 3$. As in the one-component case we assume that the interface is planar, and that the bulk nematic director is perpendicular to the interface normal. The equilibrium profiles can then be written as $\rho_\sigma(z,\theta,\varphi) = \sum_{j=0}^{N} \rho_{\sigma,j}(z,\theta)\cos(2j\varphi)$, which is the two-component analogue of equation (10). Here we restrict attention to uniaxially symmetric profiles, i.e. we ignore the φ-dependence by merely considering the $j = 0$ term in the expansion, and hence $\rho_\sigma(z,\theta) = \rho_{\sigma,0}(z,\theta)$ for $\sigma = 1, 2$. The equilibrium uniaxial profiles are solutions of

$$\log[\rho_{\sigma,0}(z,\theta)L^2 D_\sigma] + \sum_{\sigma'} \int \mathrm{d}z' \int \mathrm{d}\theta' \sin\theta' K_{00}^{\sigma\sigma'}(z-z',\theta,\theta')\rho_{\sigma',0}(z',\theta') = \beta\mu_\sigma \qquad (20)$$

where the kernels $K_{00}^{\sigma\sigma'}$ are related to the kernel K_{00} of the one-component problem by

$$K_{00}^{\sigma\sigma'}(z-z',\theta,\theta') = \frac{D_\sigma + D_{\sigma'}}{2D} K_{00}(z-z',\theta,\theta'). \qquad (21)$$

Note that the simple scaling relation (21) between the one-component and multi-component kernels only holds for rods of equal lengths; if the lengths are different the expression for $K_{00}^{\sigma\sigma'}$ is more complicated.

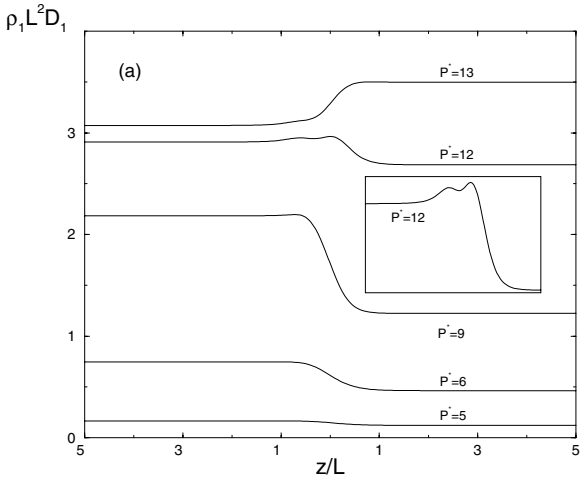

(a)

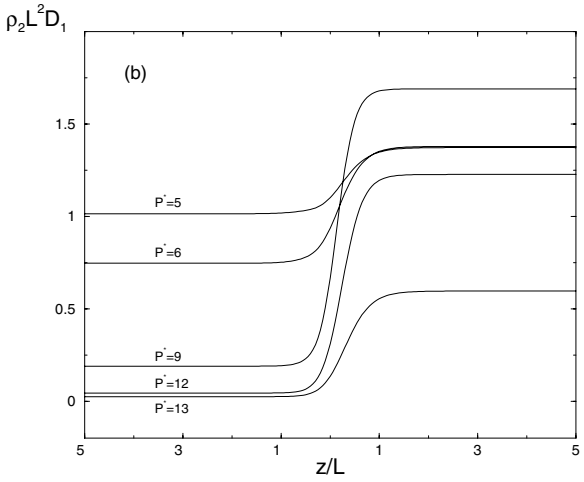

(b)

Figure 4. Profiles of the total density of thin (a) and thick (b) hard rods (diameter ratio is 3) at isotropic–nematic co-existence for several pressures p^* corresponding to the state points indicated in figure 3. The isotropic phase is at $z \to -\infty$, the nematic phase at $z \to \infty$. The profile of the thin particles is *not* always monotonic.

In order to study the IN interface of the $d = 3$ mixture we solve the minimum condition in equation (20) for the distributions $\rho_{\sigma,0}(z, \theta)$ on a $N_z \times N_\theta$ grid (z_i, θ_j), with $1 \leqslant i \leqslant N_z = 200$ and $1 \leqslant j \leqslant N_\theta = 30$, and $z_i \in [-5L, 5L]$ and $\theta_j \in [0, \pi/2]$. The chemical potentials μ_σ are chosen on the IN binodal, such that the dimensionless pressures $p^* = \beta p L^2 D_1 = 5$, 6, 9, 12, and 13. This corresponds to the state points indicated by open circles (○) in figure 3. The resulting total density profiles $\rho_\sigma(z) = \int \mathrm{d}\hat{\omega} \rho_{\sigma,0}(z, \theta)$ are shown in figure 4, where panel (a) displays the profile of the thinner species and panel (b) that of the thicker species. For $z \to -\infty$ the system is isotropic, and for $z \to \infty$ it is nematic. The first observation is that the profile for the thicker species ($\sigma = 2$) increases monotonically from a low density in the isotropic phase to a higher density in the nematic phase for all pressures p^* on the binodal.

This is not surprising given the higher total density of the nematic phase *and* the tendency of the thicker rods to reside in the nematic phase. In contrast, the total density profile of the thinner species ($\sigma = 1$) is only monotonically increasing in the pressure regime $p^* \geqslant 13$, where it is essentially a one-component system of thin rods. At lower pressure $p^* \leqslant 12$, i.e. at higher concentrations of thicker rods, $\rho_1(z)$ decreases from a higher value in the isotropic phase to a lower value in the nematic phase. Figure 4(a) reveals that this decrease is *not* necessarily monotonic, since the profiles at $p^* = 12$ (see inset) and also $p^* = 9$ show oscillatory features. The thinner rods adsorp preferentially to the interface in this pressure regime. We also studied the profile of the uniaxial order parameters $S_\sigma(z)$, but these only showed monotonic behaviour between the isotropic and nematic bulk values. The surface tension of the IN interface is shown in figure 5 as a function of the dimensionless pressure p^*, with $p^* \in [14.1/3, 14.1]$, i.e. in the pressure regime of the immiscibility gap of the bulk phase diagram of figure 3. The tension is seen to be a nonmonotonic function of p^*, with a maximum at $p^* \simeq 12$. This implies that the interface of the binary mixture is relatively stiff compared to that of the pure components. Note that the tension at $p^* = 14.1$ and $p^* = 14.1/3$ is that of the pure system, with $\beta\gamma L D_\sigma = 0.156$.

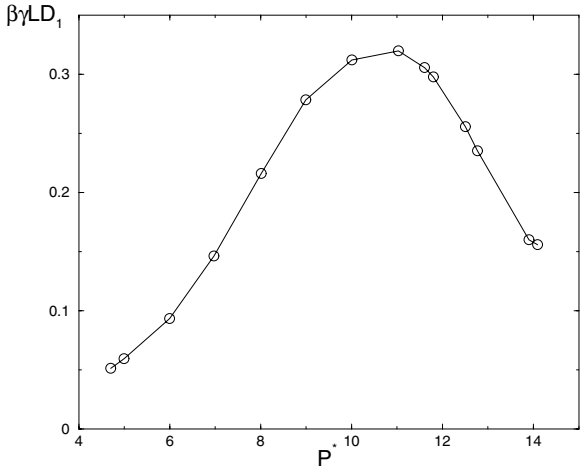

Figure 5. Surface tension of the isotropic–nematic interface of the binary thick–thin hard-rod mixture with diameter ratio 3, as a function of the dimensionless pressure $p^* \in [14.1, 14.1/3]$, i.e. the pressure regime of the immiscibility gap in the phase diagram of figure 3. The calculated points (○) are based on uniaxial profiles, i.e. $N = 1$, on a grid with $N_\theta = 30$ and $M = 5$ (see text). The numerical uncertainty is smaller than the symbols.

4. Summary and outlook

We calculated the structure and tension of the planar free interface between the co-existing isotropic and nematic phase of hard rod fluids in the Onsager limit. We restricted attention to the case where $\hat{n} \perp \hat{z}$, with $\hat{n}$ the bulk nematic director and $\hat{z}$ te interface normal. We showed that the surface tension γ of the one-component system is given by $\gamma = (0.156 \pm 0.001)kT/(LD)$, where L and D denote the length and diameter of the rods, respectively. This value is lower by about 15% than a previous estimate by Chen [7], and we argued that the difference is due to the finer spatial grids used in the present study. This conclusion is in contrast with that of [8], where a finer grid is argued to yield a higher surface tension than that of [7]. The profiles we obtain

for the total density and uniaxial order parameter are monotonic, whereas the biaxiality profile has a richer structure (see figure 2). These findings are in good agreement with those of [7], even though we treat the biaxiality perturbatively here in order to reduce the computational cost. The monotonic density and uniaxial order parameter profiles are in disagreement with the recent claims in [8].

The reduction of computational costs caused by the perturbative treatment of the interfacial biaxiality allows for a systematic study of the IN interface in binary mixtures of hard rods. We presented our first findings here for a binary mixture of thicker and thinner hard rods of the same length, with the diameter ratio of the two species equal to 3. The bulk phase diagram, shown in figure 3, is of the spindle type. Despite this simple bulk phase behaviour this system does exhibit interesting interface structure, since we found nonmonotonic density profiles at $p^* \simeq 12$ in this case. At this pressure the IN surface tension was also found to be maximal, see figure 5. We plan to extend these calculations to the IN interface of more asymmetric mixtures, where we expect new interfacial phenomena (e.g. triple-point wetting) due to presence of triple and critical points in the bulk phase diagram. We also plan to consider wetting and capillary phenomena in these systems by introducing external potentials that describe the effect of walls or substrates.

Acknowledgements

It is a pleasure to thank Marjolein Dijkstra and Jeff Chen for stimulating discussions. This work is part of the research program of the 'Stichting voor Fundamenteel Onderzoek der Materie (FOM)', which is financially supported by the 'Nederlandse organisatie voor Wetenschappelijk Onderzoek (NWO)'.

References

[1] Zocher H and Anorg Z 1925 *Chem.* **147** 91
[2] Bawden F C, Pirie N W, Bernal J D and Fankuchen I 1936 *Nature* **138** 1051
[3] Onsager L 1949 *Ann. N.Y. Acad. Sci.* **51** 627
[4] Holyst R and Poniewierski A 1988 *Phys. Rev.* A **38** 1527
[5] Moore B G and McMullen W E 1990 *Phys. Rev.* A **42** 6042
[6] Chen Z Y and Noolandi J 1992 *Phys. Rev.* A **45** 2389
[7] Chen Z Y 1993 *Phys. Rev.* E **47** 3765
[8] Koch D L and Harlen O G 1999 *Macromolecules* **32** 219
[9] Allen M 2000 *J. Chem. Phys.* **112** 5447
[10] van Roij R, Dijkstra M and Evans R 2000 *J. Chem. Phys.* **113** 7689
[11] Al-Barwani M S and Allen M P 2000 *Phys. Rev.* E **62** 6706
[12] McDonald A J, Allen M P and Schmid F 2001 *Phys. Rev.* E **63** 010 701
[13] Lekkerkerker H N W, Coulon Ph, Van Der Haegen R and Deblieck R 1984 *J. Chem. Phys.* **80** 3427
[14] Odijk Th and Lekkerkerker H N W 1985 *J.Phys. Chem.* **89** 1272
[15] Birshtein T M, Kolegov B I and Pryamitsyn V A 1988 *Polymer Science U.S.S.R* **30** 316
[16] Vroege G J and Lekkerkerker H N W 1993 *J. Phys. Chem.* **97** 3601
[17] van Roij R and Mulder B 1996 *Phys. Rev.* E **54** 6430
[18] van Roij R and Mulder B 1996 *J. Chem. Phys.* **105** 11 237
van Roij R and Mulder B 1998 *J. Chem. Phys.* **109** 1584
[19] Sear R and Jackson G 1995 *J. Chem. Phys.* **103** 8684
[20] Dijkstra M and van Roij R 1997 *Phys. Rev.* E **56** 5594
[21] van Roij R, Mulder B, Dijkstra M 1998 *Physica* A **261** 374
[22] Evans R 1979 *Adv. Phys.* **28** 143
[23] For an excellent review see e.g. Vroege G J and Lekkerkerker H N W 1992 *Rep. Progr. Phys.* **55** 1241
[24] Kayser R F and Raveché H J 1978 *Phys. Rev.* A **17** 2067
[25] Poniewierski A and Holyst R 1988 *Phys. Rev.* A **38** 3721